Stability of Ordered Phases in Diblock Copolymer Melts

Mohamed Laradji,[†] An-Chang Shi,*[,‡] Jaan Noolandi,[‡] and Rashmi C. Desai[†]

Department of Physics, University of Toronto, Toronto, Ontario, Canada M5S 1A7; and Xerox Research Center of Canada, 2660 Speakman Drive, Mississauga, Ontario, Canada L5K 2L1

Received December 13, 1996; Revised Manuscript Received March 27, 1997[⊗]

ABSTRACT: The stability of the diblock copolymer ordered phases is investigated by means of a novel theory of anisotropic composition fluctuations. The analogy between a polymer chain in a periodic structure and an electron in a crystalline solid is exploited in the development of the theory. This theory allows the calculation of the spinodal lines, the most unstable modes, and the scattering functions of the ordered phases. The one-phase regions of the lamellar, cylindrical, and spherical phases are found to be within their corresponding stability regions. On the other hand, the hexagonally-perforated lamellar phase is unstable along the lamellar−cylindrical phase boundary. The most unstable fluctuation modes are readily identified and are used to infer the kinetic pathways of the order−order phase transitions. We speculate that the experimentally observed modulated and/or perforated layered states along the lamellar−cylindrical phase boundary are a consequence of the infinitely degenerate fluctuation modes of the lamellar phase. The scattering functions of all ordered phases are calculated. The stability of the double gyroid phase is also investigated.

I. Introduction

A−B diblock copolymers are long polymer chains composed of two incompatible blocks. The incompatibility between the two blocks drives the system to phase separation at low temperature. However, the fact that the A−B blocks are chemically connected prevents macroscopic phase separation. The phase separation of the diblock copolymer melt is, therefore, necessarily on a length scale dictated by the chain length, leading to microphases with A- and B-rich domains separated by internal interfaces. The competition between the spontaneous curvature of the internal interfaces and the entropic stretching of the polymer chains determines the symmetry of the equilibrium phases. Diblock copolymer melts are found to self-assemble into a variety of ordered microphases, and the rich phase behavior of this amphiphilic system has attracted a lot of attention.[1,2] Such complex self-assembly is shared by many other complex fluids such as microemulsions and Langmuir monolayers.[3]

Diblock copolymers are characterized by the degree of polymerization, Z, and the volume fraction of the A-monomers, f. The interaction between the monomers is characterized by the Flory−Huggins parameter, χ. Traditionally, the phase diagram of a diblock copolymer melt is specified by the parameters χZ and f. The segregation between the two blocks is dictated by χZ whereas the interfacial curvature is controlled by f. At low χZ (high temperatures) a diblock copolymer melt is homogeneous. An order−disorder transition occurs when χZ is increased.[4] For symmetric copolymers with $f = 0.5$, the melt is ordered into a lamellar (L) structure. As f is increased or decreased, a cylindrical (C) phase and then a spherical (S) phase are usually observed. Besides these three classical phases, three additional complex structures corresponding to hexagonally-modulated or perforated layers (HML/HPL),[5] and a double-gyroid (DG) phase with space group $Ia\bar{3}d$[6] have been identified in a narrow range of f and χZ separating the lamellar and cylindrical phases.[2] Earlier studies have contributed to the understanding of many of the equilibrium aspects of diblock copolymer phase diagram and the morphologies of the ordered phases. However, the thermodynamic stability of the ordered phases and the dynamical process through which they emerge remain relatively unexplored.[7] Hajduk *et al.*[8] observed that the lamellar to cylindrical transition proceeds via an intermediate modulated layered state. On the other hand, experiments by Sakurai *et al.*[9,10] on ABA triblock copolymers indicate that the cylinders transform into a lamellar structure directly. Recently Hajduk *et al.*[11] have shown that the HML and HPL morphologies are long-lived nonequilibrium states when the melt is driven away from the lamellar phase.

Theoretically, the phase behavior of diblock copolymer melts has been studied using mean-field theory, and a recent theoretical review is given by Matsen and Bates.[12] The mean-field calculations have been successful in predicting the appearance of the three classical phases in diblock copolymer melts. The DG phase is also predicted to occur in a narrow region along the L−C phase boundary extending from a triple point at $\chi Z \approx 11.14$ to larger χZ. On the other hand, the HML/HPL phases are found to be metastable phases. We emphasize that, due to the neglect of composition fluctuations, the self-consistent mean-field theory cannot address the thermodynamic stability of the ordered phases. In order to analyze the stability of the ordered phase in diblock copolymers, a proper treatment of the *anisotropic* composition fluctuations is necessary. The first theory which treated the composition fluctuations in diblock copolymer melts is due to Fredrickson and Helfand,[13] who extended Brasovskii theory[14] to diblock copolymers. In the theory of Fredrickson and Helfand, the Landau free energy functional of Leibler[4] was reduced to a form considered by Brasovskii, and then a saddle-point approximation (*i.e.*, the self-consistent Hartree approximation) was performed for the fluctuations. However, this theory is confined to the weak segregation region due to its use of the Landau free energy functional. The theory was later extended by Mayes and

[†] University of Toronto.
[‡] Xerox Research Center of Canada.
[⊗] Abstract published in *Advance ACS Abstracts,* May 15, 1997.

S0024-9297(96)01843-8 CCC: $14.00

Olvera de la Cruz[15] to include the leading wave vector dependence of the vertex functions but keeping the saddle-point approximation and remaining in the weak segregation limit. More recently, Muthukumar[16] studied composition fluctuation effects on the phase diagram of diblock copolymer melts through the incorporation of composition fluctuations into a density functional theory. However, the chain conformations are treated approximately in this theory due to the truncated form of the free energy functional. It is important to remark that the fluctuation theories, cited above, are characterized by the isotropic correlation functions which are derived from Leibler's theory.[4] Recently, we have developed a theory for anisotropic fluctuations in ordered phases of diblock copolymer melts by means of a self-consistent expansion around the *exact* mean-field solution. The lowest correction to the mean-field approximation is in the form of Gaussian fluctuations around the mean-field solution. These fluctuations are characterized by the anisotropic density−density correlation functions. The theory has been applied to the simple lamellar phase.[17] A description of the theoretical framework and the nature of the anisotropic fluctuations is given in an earlier publication.[18] In the present paper, the theory for anisotropic fluctuations is developed into a convenient scaled form and then applied to all ordered phases in diblock copolymer melts in the weak segregation limit. Some of our results were recently reported by us in a brief communication.[19]

The main thrust of the theory is that, in order to study the effect of fluctuations in an *ordered broken-symmetry* phase, a self-consistent expansion must be performed around the *exact* mean-field solution. The chain conformations are therefore described by those of a flexible chain in a periodic potential, *i.e.*, by a diffusion equation in a periodic potential. Since in quantum mechanics the Schrödinger equation is a diffusion equation with imaginary time, the chain conformation problem is equivalent to the problem of an electron in a periodic potential. Therefore, the theory bears an important and useful analogy with the theory of energy bands in crystalline solids. This analogy enables us to exploit the symmetry of the ordered phases and to use many techniques developed in solid state physics.[20] In this paper, we present results on the scattering functions, the spinodal lines, and the least stable or most unstable modes of the ordered phases in diblock copolymer melts. In particular, we show that the HPL phase is unstable along the lamellar−cylindrical phase boundaries, in accordance with the recent experiments of Hajduk *et al.*[11] The least-stable or most-unstable fluctuation modes are used to infer information on the kinetic pathway of the order−order phase transitions and the epitaxial relations between the different ordered phases, leading to results which are in good agreement with experiments and the recent kinetic study of Qi and Wang[21] using a time-dependent Ginzburg−Landau theory.

The structures of the ordered phases of diblock copolymers are mostly identified from the scattering intensities, which are obtained from small-angle X-ray or neutron scattering. The scattering function of the homogeneous phase was calculated for the first time by Leibler.[4] However, the theoretical calculation of the scattering functions for ordered diblock copolymer phases has been lacking. While the calculation of the scattering functions for the lamellar phase has been given in an earlier paper,[17] the scattering functions of all ordered phases are given in the present paper.

The paper is organized as follows. A brief account of the theory for diblock copolymer melts is given in section II. The theory of anisotropic fluctuations and its reciprocal space formulation is presented in section III. The results on the three classical phases (lamellar, cylindrical, and spherical) are given in section IV, and those on the two recently identified complex phases, *i.e.*, the HPL and the DG phases, are presented in sections V and VI, respectively. Finally, the last section is devoted to concluding remarks. Some of the details of the theory and the numerical techniques are given in Appendices A and B.

II. Theory of Diblock Copolymer Melts

For the study of the diblock copolymer phase behavior, we adopt the "standard" model in which the hard-core monomer−monomer interaction is modeled by an incompressibility constraint and the polymer chains are assumed to be fully flexible. We consider N polymer chains in a volume V. A single polymer chain consists of an A−block and a B-block, each consisting of $f_\alpha Z$ statistical segments, where $f_\alpha = f$ or $1 - f$ for α = A or B, respectively. We will use the convention in which all lengths are scaled by the Gaussian radius of gyration, $R_g = b(Z/6)^{1/2}$, where b is the monomer statistical Kuhn length (we consider the case where the A- and B-monomers have the same size) and the chain arc length is scaled by the chain degree of polymerization Z. The local volume fraction is used as a collective variable,

$$\phi_\alpha(\mathbf{r}) = \frac{1}{\rho_0}\sum_{i=1}^{N}\int_0^{f_\alpha} d\tau\, \delta(\mathbf{r} - \mathbf{r}_i^\alpha(\tau)) \tag{1}$$

where ρ_0 is the number density of the melt and $\{r_i^\alpha(\tau)\}$ describes the chain conformations. The partition function of the standard model is given by

$$Z = \int\prod_{i=1}^{N} D\mathbf{r}_i(\tau)\mathrm{P}(\{\mathbf{r}_i(\tau)\})\prod_{\mathbf{r}}\delta[1 - \sum_\alpha \phi_\alpha(\mathbf{r})] \times \exp\left[-\frac{\rho_0 R_g^3}{Z}\int d\mathbf{r}\, \chi Z\phi_A(\mathbf{r})\,\phi_B(\mathbf{r})\right] \tag{2}$$

where the δ-function accounts for the incompressibility constraint. The connectivity of the monomers within each chain is ensured through the functional P, which, for fully flexible diblock copolymers, is given by

$$\mathrm{P}(\{\mathbf{r}(\tau)\}) = \prod_{i=1}^{N}\delta[\mathbf{r}_i^A(f_A) - \mathbf{r}_i^B(f_B)]\prod_\alpha \exp\left[-\frac{3}{2b^2}\int_0^{f_\alpha} d\tau \left(\frac{d\mathbf{r}_i^\alpha(\tau)}{d\tau}\right)^2\right] \tag{3}$$

The functional integration over the chain conformations is replaced by a functional integration over the local volume fractions and two auxiliary fields, ω_A and ω_B[22]

$$Z = \int\prod_\alpha \{D\phi_\alpha D\omega_\alpha\}\prod_r \delta[\sum_\alpha \phi_\alpha(\mathbf{r}) - 1]\exp[-F(\{\phi_\alpha\},\{\omega_\alpha\})] \tag{4}$$

where the free energy functional F is given by

$$F(\{\phi_\alpha\},\{\omega_\alpha\}) = \frac{\rho_0 R_g^3}{Z}\{\int d\mathbf{r}\,[\chi Z\phi_A(\mathbf{r})\,\phi_B(\mathbf{r}) - \sum_\alpha \omega_\alpha(\mathbf{r})\,\phi_\alpha(\mathbf{r})] - V\ln Q_c(\{\omega_\alpha\})\} \tag{5}$$

$Q_c(\{\omega_\alpha\})$ is the partition function of an independent single

chain subject to the field ω_α. It can be written as a product of two propagators

$$Q_c(\{\omega_\alpha\}) = \frac{1}{V}\int d\mathbf{r}_1\, d\mathbf{r}_2\, d\mathbf{r}_3\, Q_A(\mathbf{r}_1,f_A|\mathbf{r}_2)\, Q_B(\mathbf{r}_2,f_B|\mathbf{r}_3) \quad (6)$$

where $\mathbf{r}_1$, $\mathbf{r}_3$, and $\mathbf{r}_2$ are the positions of the free ends of the A-block, the B-block, and the junction, respectively. The propagator $Q_\alpha(\mathbf{r},t|\mathbf{r}')$ satisfies the following modified diffusion equation[23]

$$\frac{\partial}{\partial t}Q_\alpha(\mathbf{r},t|\mathbf{r}') = \nabla^2 Q_\alpha(\mathbf{r},t|\mathbf{r}') - \omega_\alpha(\mathbf{r})\, Q_\alpha(\mathbf{r},t|\mathbf{r}') \quad (7)$$

with the boundary condition $Q_\alpha(\mathbf{r},0|\mathbf{r}') = \delta(\mathbf{r}-\mathbf{r}')$.

In principle, all thermodynamic information can be extracted from the partition function Z. However, methods of evaluating the functional integral exactly have not been developed. Therefore, a variety of approximations have to be adopted. In particular, evaluating the partition function (eq 4) by the saddle-point approximation leads to the widely used self-consistent mean-field theory. The mean-field theory describes the interacting chains by an ensemble of independent chains in the self-consistent mean fields created by all other chains. Mathematically, the saddle-point method corresponds to the extremization of the free energy functional (eq 5), resulting in the following mean-field equations

$$\omega_\alpha^{(0)}(\mathbf{r}) = \chi Z \phi_\beta^{(0)}(\mathbf{r}) + \eta(\mathbf{r}) \quad (8)$$

$$\phi_\alpha^{(0)}(\mathbf{r}) = \frac{1}{Q_c^{(0)}}\int_0^{f_\alpha} dt \int d\mathbf{r}_1\, d\mathbf{r}_2\, d\mathbf{r}_3\, Q_\alpha^{(0)}(\mathbf{r}_1,t|\mathbf{r}) \times Q_\alpha^{(0)}(\mathbf{r},f_\alpha-t|\mathbf{r}_2)\, Q_\beta^{(0)}(\mathbf{r}_2,f_\beta|\mathbf{r}_3) \quad (9)$$

where the field $\eta(\mathbf{r})$ is a local Lagrange multiplier which is introduced to enforce the incompressibility condition, $\sum_\alpha \phi_\alpha^{(0)}(\mathbf{r}) = 1$. The mean-field propagator, $Q_\alpha^{(0)}(\mathbf{r},t|\mathbf{r}')$, satisfies the modified diffusion equation

$$\frac{\partial}{\partial t}Q_\alpha^{(0)}(\mathbf{r},t|\mathbf{r}') = \nabla^2 Q_\alpha^{(0)}(\mathbf{r},t|\mathbf{r}') - \omega_\alpha^{(0)}(\mathbf{r})\, Q_\alpha^{(0)}(\mathbf{r},t|\mathbf{r}') \quad (10)$$

We notice that the parameters entering the mean-field theory are combinations of χZ and f. Therefore, the use of these two parameters for describing the phase diagram is justified within the mean-field approximation. Because of the complexity of the theory even within mean-field approximation, a variety of further approximations have been adopted to solve the mean-field equations. To obtain an exact solution, the mean-field theory is reformulated in reciprocal space in order to exploit the full symmetries of the ordered structures.[24] In this reciprocal space method, the mean-field quantities are expanded in terms of plane waves. The mean-field phase diagram is then obtained by comparing the free energies of all structures. Whereas the self-consistent equations ensure that the free energy is extremized, they do not necessarily ensure its minimization. It is therefore possible that a given mean-field solution corresponds to a saddle point.

In order to investigate the stability of the ordered phases, we have to include the effect of fluctuations in the theory. In this paper we study the effect of composition fluctuations at the Gaussian level. Let $\delta\phi_\alpha(\mathbf{r})$ and $\delta\omega_\alpha(\mathbf{r})$ be the local fluctuations of $\phi_\alpha(\mathbf{r})$ and $\omega_\alpha(\mathbf{r})$ away from their mean-field values, $\phi_\alpha^{(0)}(\mathbf{r})$ and $\omega_\alpha^{(0)}(\mathbf{r})$, respectively. After carrying out the expansion in terms of the fluctuating fields, the free energy functional (eq 5) is written as[18]

$$F = F^{(0)} + F^{(1)} + F^{(2)} \ldots \quad (11)$$

where $F^{(0)}$ is the mean-field free energy, $F^{(1)} = 0$ because the mean-field solution extremizes the free energy functional given by eq 5, and the second-order Gaussian correction is given by

$$F^{(2)}(\{\delta\phi_\alpha\},\{\delta\omega_\alpha\}) = \frac{\rho_0 R_g^3}{Z}\Big\{\int d\mathbf{r}\, [\chi Z\, \delta\phi_A(\mathbf{r})\, \delta\phi_B(\mathbf{r}) - \sum_\alpha \delta\omega_\alpha(\mathbf{r})\, \delta\phi_\alpha(\mathbf{r})] - \frac{1}{2}\sum_{\alpha\beta}\int d\mathbf{r} \int d\mathbf{r}'\, C_{\alpha\beta}(\mathbf{r},\mathbf{r}')\, \delta\omega_\alpha(\mathbf{r})\, \omega_\beta(\mathbf{r}')\Big\} \quad (12)$$

Higher order corrections are explicitly functionals of $\delta\omega_\alpha$ only. The two-point cumulants in eq 12, $C_{\alpha\beta}(\mathbf{r},\mathbf{r}')$, are completely determined by the mean- field propagators and are given by

$$C_{AA}(\mathbf{r},\mathbf{r}') = \frac{1}{Q_c^{(0)}}\int_0^{f_A} dt \int_0^t dt' \int d\mathbf{r}_1\, d\mathbf{r}_2\, d\mathbf{r}_3\, [Q_A^{(0)}(\mathbf{r}_1,f_A-t|\mathbf{r}) \times Q_A^{(0)}(\mathbf{r},t-t'|\mathbf{r}')\, Q_A^{(0)}(\mathbf{r}',t'|\mathbf{r}_2)\, Q_B^{(0)}(\mathbf{r}_2,f_B|\mathbf{r}_3) + Q_A^{(0)}(\mathbf{r}_1,f_A-t|\mathbf{r}') \times Q_A^{(0)}(\mathbf{r}',t-t'|\mathbf{r})\, Q_A^{(0)}(\mathbf{r},t'|\mathbf{r}_2)\, Q_B^{(0)}(\mathbf{r}_2,f_B|\mathbf{r}_3)] \quad (13)$$

and

$$C_{AB}(\mathbf{r},\mathbf{r}') = \frac{1}{Q_c^{(0)}}\int_0^{f_A} dt \int_0^{f_B} dt' \int d\mathbf{r}_1\, d\mathbf{r}_2\, d\mathbf{r}_3\, Q_A^{(0)}(\mathbf{r}_1,f_A-t|\mathbf{r}) \times Q_A^{(0)}(\mathbf{r},t|\mathbf{r}_2)\, Q_B^{(0)}(\mathbf{r}_2,t'|\mathbf{r}')\, Q_B^{(0)}(\mathbf{r}',f_B-t'|\mathbf{r}_3) \quad (14)$$

with $C_{BB}(\mathbf{r},\mathbf{r}')$ and $C_{BA}(\mathbf{r},\mathbf{r}')$ obtained by exchanging A and B in eqs 13 and 14, respectively. If we truncate the fluctuations at the Gaussian level, the partition function of the melt is approximated by

$$Z \approx \exp(-F^{(0)})\int D\, \delta\phi_\alpha\, D\, \delta\omega_\alpha \prod_r \delta\Big(\sum_\alpha \delta\phi_\alpha(\mathbf{r})\Big) \times \exp(-F^{(2)}(\{\delta\phi_\alpha\},\{\delta\omega_\alpha\})) \quad (15)$$

Because of the incompressibility constraint, the fluctuations in the compositions are not independent. We thus introduce a new collective variable $\delta\phi(\mathbf{r}) = \delta\phi_A(\mathbf{r}) - \delta\phi_B(\mathbf{r})$ to describe the composition fluctuations. It is desirable to obtain an effective free energy functional in terms of $\delta\phi$ only. This can be achieved by performing the functional integral over $\delta\omega_A$ and $\delta\omega_B$ in eq 15, leading to the effective free energy functional

$$F^{(2)}(\{\delta\phi\}) = \frac{1}{2}\int d\mathbf{r}\, d\mathbf{r}'\, [C^{RPA}]^{-1}(\mathbf{r},\mathbf{r}')\, \delta\phi(\mathbf{r})\, \delta\phi(\mathbf{r}') \quad (16)$$

where the two-point density−density correlation function can be written in the following matrix form

$$\mathbf{C}^{RPA} = \frac{\rho_0 R_g^3}{Z}\Big[\mathbf{I} - \frac{\chi Z}{2}\tilde{\mathbf{C}}\Big]^{-1}\cdot\tilde{\mathbf{C}} \quad (17)$$

where $\mathbf{I}$ is the identity matrix and $\tilde{\mathbf{C}} = \mathbf{C} - \Delta_1\cdot\Sigma^{-1}\cdot\Delta_2$. The operators $\mathbf{C}$, Σ, Δ_1, and Δ_2 are combinations of the two-point cumulants, $\mathbf{C}_{\alpha\beta}$:

$$\mathbf{C} = \mathbf{C}_{AA} - \mathbf{C}_{AB} - \mathbf{C}_{BA} + \mathbf{C}_{BB}$$

$$\Delta_1 = \mathbf{C}_{AA} + \mathbf{C}_{AB} - \mathbf{C}_{BA} - \mathbf{C}_{BB}$$

$$\Delta_2 = \mathbf{C}_{AA} - \mathbf{C}_{AB} + \mathbf{C}_{BA} - \mathbf{C}_{BB}$$

$$\Sigma = \mathbf{C}_{AA} + \mathbf{C}_{AB} + \mathbf{C}_{BA} + \mathbf{C}_{BB} \quad (18)$$

It should be noted that, in general, the integration of $\delta\omega_\alpha$ cannot be carried out exactly, and a random-phase approximation (RPA) is usually adopted. This corresponds to a mean-field approximation for the $\delta\omega_A$ and $\delta\omega_B$, while keeping $\delta\phi$ fixed. At the Gaussian level, such an approximation is exact.

Integrating out the composition fluctuations leads to the partition function

$$Z \approx \exp(-F^{(0)})\left\{\det\left[\left(\frac{\rho_0 R_g^3}{2\pi Z}\right)^3\left(\mathbf{I} - \frac{\chi Z}{2}\tilde{\mathbf{C}}\right)\cdot\Sigma\right]\right\}^{-1/2} \quad (19)$$

It is important to emphasize that the mean-field solution and the two-point cumulants are functions of the two parameters χZ and f only. The inclusion of fluctuations introduces a third parameter, $\bar{Z} = \rho_0^2 R_g^6/Z^2 = (\rho_0^2 b^6/6^3)Z$, which quantifies fluctuation effects. This is in accordance with previous studies.[13]

The density−density correlation function, $C^{\mathrm{RPA}}(\mathbf{r},\mathbf{r}')$, can be used to obtain information about several important thermodynamic properties: (1) The mean-field solution for a given phase is linearly stable when all the eigenvalues of $\mathbf{C}^{\mathrm{RPA}}$ are positive. The boundary in the $(\chi Z,f)$ plane where the smallest eigenvalue becomes zero defines the spinodal line for that phase. (2) The experimentally observed scattering intensities correspond to the Fourier transform of $C^{\mathrm{RPA}}(\mathbf{r},\mathbf{r}')$. Our theory accounts for anisotropic fluctuations and therefore enables us to calculate the scattering functions of the periodic ordered phases. (3) The elastic moduli of the ordered phases can be extracted from the scattering functions, as demonstrated earlier by Yeung *et al.*[17]

III. Reciprocal Space Theory of Anisotropic Fluctuations

The theory developed above is formulated in real space. However, calculating the density−density correlation within this formalism can be carried out only for very simple geometries, such as the lamellar phase.[17] In order to apply the theory to the more complex phases, novel methods other than the direct real space calculation have to be developed. In particular, the full symmetries of the ordered phases can be exploited to cast the theory into a tractable form. The key observation in this problem is that the mean-field solution is periodic, and the modified diffusion equation for the chain propagator is equivalent to the Shrödinger equation of an electron in a crystalline solid with the Hamiltonian $H_\alpha = -\nabla^2 + \omega_\alpha^{(0)}(\mathbf{r})$. It is well-known from solid-state physics that the electronic energy in a crystal forms bands according to Bloch's theorem;[20] *i.e.*, the eigenmodes of H_α can be labeled by the band index, n, and a reduced wave vector, $\mathbf{k}$, within the first Brillouin zone. The normalized eigenfunctions of H_α are Bloch functions of the form

$$\psi_{n\mathbf{k}}^\alpha(\mathbf{r}) = \frac{1}{\sqrt{V}}\sum_{\mathbf{G}} u_{n\mathbf{k}}^\alpha(\mathbf{G})\mathrm{e}^{i(\mathbf{k}+\mathbf{G})\cdot\mathbf{r}} \quad (20)$$

where the set $\{\mathbf{G}\}$ constitutes the reciprocal lattice vectors. The coefficients $u_{n\mathbf{k}}^\alpha(\mathbf{G})$ are solutions of the following set of linear equations

$$[(\mathbf{k}+\mathbf{G})^2 - \epsilon_{n\mathbf{k}}^\alpha]u_{n\mathbf{k}}^\alpha(\mathbf{G}) + \sum_{\mathbf{G}'}\omega^\alpha(\mathbf{G}-\mathbf{G}')u_{n\mathbf{k}}^\alpha(G') = 0 \quad (21)$$

where $\omega_\alpha(\mathbf{G})$ are the Fourier components of the auxiliary mean fields; *i.e.*, $\omega_\alpha^{(0)}(\mathbf{r}) = \Sigma_{\mathbf{G}}\omega^\alpha(\mathbf{G})\exp(i\mathbf{G}\cdot\mathbf{r})$. In principle, this eigenvalue problem has an infinite dimension, but since the coefficients $\omega^\alpha(\mathbf{G})$ are very small for large reciprocal wave vectors, the coefficients can be truncated at a finite number N, leading to an $N \times N$ eigenvalue problem. The solution of this problem can be carried out using standard linear algebra software packages. A generic feature of the eigenvalues of H_α is the presence of band gaps at the zone boundaries. Figure 1 shows the low-index eigenvalue bands for the lamellar and homogeneous phases, at $\chi Z = 11$ and $f = 0.5$. It is obvious from this figure that the band gaps appear only because of a finite periodic ω_α.

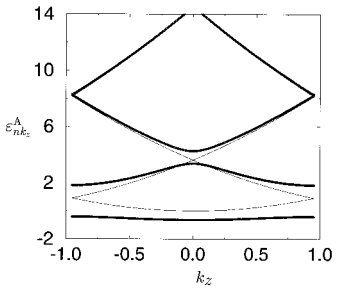

Figure 1. Eigenvalues $\epsilon^{\mathrm{A}}_{n,\mathbf{k}z}$ of the chain Hamiltonian H_{A} for the lamellar phase (thick lines) and the homogeneous phase $\omega_{\mathrm{A}}(\mathbf{r}) = 0$ (thin lines) at $\chi Z = 11$ and $f = 0.5$. Notice that the broken symmetry of the lamellar phase leads to the formation of band gaps which are not present for the homogeneous case.

Because the eigenfunctions of H_α form a complete orthogonal basis, they can be used for the expansion of the fluctuating fields. The explicit expressions of the two-point cumulants are found in Appendix A. In particular, $C_{n,n'}^{\alpha\beta}(\mathbf{k},\mathbf{k}')$ becomes diagonal in $\mathbf{k}$-space due to the constraint of the wave vectors $\mathbf{k}$ within the first Brillouin zone. These two-point cumulants become $N \times N$ matrices at each wave vector $\mathbf{k}$. Since $\mathbf{C}^{\mathrm{RPA}}$ is a combination of these two-point cumulants, it becomes diagonal in $\mathbf{k}$. Thus finding the eigenvalues of $\mathbf{C}^{\mathrm{RPA}}$ becomes an $N \times N$ eigenvalue problem at each reduced wave vector $\mathbf{k}$.

Our study of the stability of an ordered phase proceeds as follows:

(1) The mean-field solution at a certain point of the phase diagram, $(\chi Z, f)$, is obtained by solving the self-consistent equations, eqs 8−10, in reciprocal space. In particular, the mean-field phase diagram which we have calculated is in complete agreement with the ealier work of Matsen and Schick.[24] Details of the mean-field calculations are found in Appendix B. The mean-field calculations are used to obtain the phase diagram at weak segregations and to provide the Fourier components $\omega_\alpha(\mathbf{G})$ needed for the fluctuations calculation.

(2) The mean-field Fourier components of $\omega_\alpha(\mathbf{G})$ are then used to construct the Hamiltonian H_α. The eigenvalues $\epsilon_{n\mathbf{k}}$ and the components of their corresponding eigenvectors $u_{n\mathbf{k}}^\alpha(\mathbf{G})$ are then calculated by solving the set of linear equations, eq 21, at the wave vectors, $\mathbf{k}$, which are constrained within the first Brillouin zone. We exploit the symmetries of the first Brillouin zone by considering only a portion of the Brillouin zone, which is then discretized into a fine mesh.

(3) The eigenvalues, $\epsilon_{n\mathbf{k}}^\alpha$, and eigenvectors, $u_{n\mathbf{k}}^\alpha$, are then used to construct the matrix elements of $C_{n,n'}(\mathbf{k})$ using their expressions, eqs A1−A4, in Appendix A.

(4) The eigenvalues of $\mathbf{I} - (\chi Z/2)\tilde{\mathbf{C}}$ are calculated using eqs 17 and 18.

(5) The stability of the structure is investigated by examining the eigenvalues of $\mathbf{I} - (\chi Z/2)\tilde{\mathbf{C}}$ (the eigenvalues of Σ are always positive). If all the eigenvalues are positive, the phase is linearly stable or metastable. However, if at least one eigenvalue is negative, the phase is linearly unstable. The boundary between the metastable and the unstable regions defines the spinodal line. For illustration, Figure 2 displays the eigenvalues, $\lambda_{n\mathbf{k}}$ of $\mathbf{I} - (\chi Z/2)\tilde{\mathbf{C}}(\mathbf{k})$ for the lamellar phase at $\chi Z = 10.8$ and $f = 0.46$ along the path ΓM on the q_z-axis (the lamellae are perpendicular to the x-axis) and along the path $M\,XY$, *i.e.* along the edge of the first Brillouin zone. The important observation which can

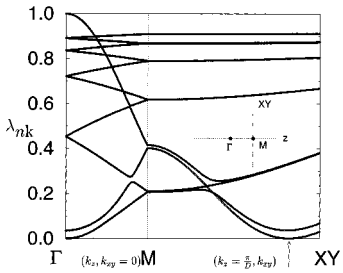

Figure 2. Plot of the eigenvalues of the operator $\mathbf{C}^{\mathrm{RPA}}$, $\lambda_{n\mathbf{k}}$, for the lamellar phase in the first Brillouin zone at $\chi Z = 10.8$ and $f = 0.46$. The paths Γ*M* and *MXY* are shown by the inset of the figure. The arrow indicates where the smallest eigenvalue occurs. Notice that the instability occurs at the edge of the Brillouin zone ($k_z = \pi/D$ and a finite k_{xy} (arrow)). At this point of the phase diagram the lamellar phase is almost unstable. As is discussed in the text, this corresponds to an instability of the lamellar phase against an intermediate modulated-layered state.

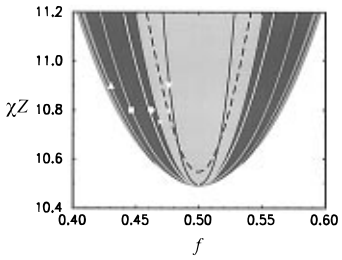

Figure 3. Phase diagram of diblock copolymer melts and the spinodal lines. The shaded regions correspond to the one-phase regions of the lamellar (light gray), cylindrical (dark gray), and spherical (medium gray) phases. The spinodal lines of the ordered phases are shown by their corresponding gray levels. The spinodal line of the hexagonally perforated lamellar phase is indicated by the broken line. The white region corresponds to the homogeneous phase. The outer spinodal line of the spherical phase is not obtained due to numerical difficulties in finding unstable mean-field solutions of the spherical structure within the homogeneous one-phase region. The various symbols correspond to the points of the phase diagram at which the scattering functions and the real space profiles of the various phases are calculated.

be made from this figure is that the most unstable eigenmode occurs at the first Brillouin zone boundaries, in accordance with the earlier calculations of Shi *et al.* using perturbation theory.[18]

We now turn to the calculation of the scattering functions within our theoretical framework. The experimentally observed scattering intensity is proportional to the Fourier transform of the density−density correlation function,

$$I(\mathbf{q}) = \frac{1}{V}\int \mathrm{d}\mathbf{r}_1\, \mathrm{d}\mathbf{r}_2\, \mathrm{e}^{-\mathbf{q}\cdot(\mathbf{r}_1-\mathbf{r}_2)}\langle\phi(\mathbf{r}_1)\phi(\mathbf{r}_2)\rangle \tag{22}$$

where $\phi(\mathbf{r}) = \phi_{\mathrm{A}}(\mathbf{r}) - \phi_{\mathrm{B}}(\mathbf{r})$. For an ordered phase,

$$\phi(\mathbf{r}) = \sum_{\mathbf{G}} \phi^{(0)}(\mathbf{G})\mathrm{e}^{i\mathbf{G}\cdot\mathbf{r}} + \delta\phi(\mathbf{r}) \tag{23}$$

Inserting this form into eq 22, the scattering intensity becomes

$$I(\mathbf{q}) = \sum_{\mathbf{G}} |\phi^{(0)}(\mathbf{G})|^2 \delta_{\mathbf{q},\mathbf{G}} + S(\mathbf{q}) \tag{24}$$

where $S(\mathbf{q})$ is the scattering function due to composition fluctuations and is given by

$$S(\mathbf{q}) = \frac{1}{V}\int \mathrm{d}\mathbf{r}_1\, \mathrm{d}\mathbf{r}_2\, \mathrm{e}^{-\mathbf{q}\cdot(\mathbf{r}_1-\mathbf{r}_2)}\langle\delta\phi(\mathbf{r}_1)\,\delta\phi(\mathbf{r}_2)\rangle \tag{25}$$

Therefore, the scattering intensity is composed of two contributions: The first one corresponds to a set of Bragg peaks located at the reciprocal wave vectors, whose amplitudes are completely determined by the mean-field solution. The second contribution is due to composition fluctuations and has to be calculated from a theory of fluctuations. The pair-correlation function of the density fluctuations is the RPA correlation function which can be expanded in terms of the Bloch eigenfunctions

$$\langle\delta\phi(\mathbf{r})\,\delta\phi(\mathbf{r}')\rangle = C^{\mathrm{RPA}}(\mathbf{r},\mathbf{r}') = \sum_{\mathbf{k}}\sum_{n,n'} C^{\mathrm{RPA}}_{nn'}(\mathbf{k})\,\Psi^{\mathrm{A}*}_{n\mathbf{k}}(\mathbf{r})\,\Psi^{\mathrm{A}}_{n'\mathbf{k}}(\mathbf{r}') \tag{26}$$

Using this form, the scattering function is given by

$$S(\mathbf{q}) = \sum_{\mathbf{G}}\sum_{nn'} C^{\mathrm{RPA}}_{nn'}(\mathbf{q}-\mathbf{G}) u^{\mathrm{A}*}_{n,\mathbf{q}-\mathbf{G}}(\mathbf{G})\, u^{\mathrm{A}}_{n',\mathbf{q}-\mathbf{G}}(\mathbf{G}) \tag{27}$$

IV. Stability, Scattering Functions, and Fluctuation Modes

In this section we present results on the stability, the scattering functions, and the fluctuation modes of the ordered phases in diblock copolymer melts. We concentrate on the weak segregation region, where fluctuations are most significant; most of our analyses are confined to the region defined by $\chi Z < 11.2$. Within mean-field theory, the lamellar, cylindrical, and spherical phases are stable in this region. On the other hand, the HPL phase is found to be metastable within this region.[24] Our results on the more complex case corresponding to the double-gyroid phase, which appears above a triple point located at $\chi Z = 11.14$,[24] will be presented in section VI.

The results of the stability analysis of the lamellar, cylindrical, spherical, and HPL structures are summarized in the generalized phase diagram of Figure 3. In this figure, the mean-field one-phase regions of the lamellar, cylindrical, and spherical phases are indicated by the shaded light-gray, dark-gray, and medium-gray areas, respectively. The spinodal lines of these phases are shown by lines with their corresponding gray levels. The HPL structure is metastable within its spinodal line, shown by the broken line. The most significant aspect of this phase diagram is that the one-phase regions of the so-called classical phases are encapsulated within their spinodals, indicating the robustness of these three phases which are easily observed in experiments. On the other hand, the HPL phase is metastable in the center of the lamellar one-phase region and is unstable in the rest of the phase diagram. Therefore, the HPL phase is thermodynamically unstable along the lamellar−cylindrical phase boundary, where it has been identified in several experiments. We will argue below that the experimentally observed modulated layered states are simply an intermediate structure due to the infinitely degenerate fluctuation modes of the lamellar phase. Another interesting feature of this phase diagram is that the cylindrical and spherical phases have two symmetrically unrelated spinodal lines, whereas the lamellar and the HPL phases have two symmetrically related spinodal lines. This is due to the fact the majority and the minority domains of the lamellar and HPL phases are topologically equivalent (the HPL structure being bicontinuous). In the rest of this section, we will present details of the scattering functions and the fluctuation modes leading to the instability of the phases, which are used to infer the kinetic pathways of the order−order transitions and the epitaxial relations between the various structures.

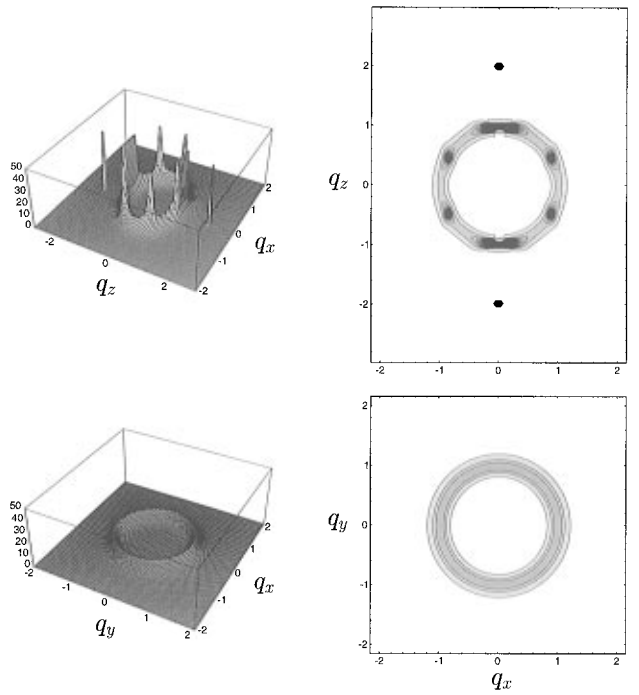

Figure 4. Scattering function of the lamellar phase at $\chi Z = 10.8$, $f = 0.462$ prior to its spinodal line (shown by the symbol ○ in Figure 3). The two cuts, corresponding to the q_x-q_z plane and the q_x-q_y plane, are shown in the top part and the bottom part, respectively. The two left graphs show the surface plots of the structure factor, and the two right graphs correspond to their contour plots. Notice that the q_y direction in the upper part of this figure could be any in-plane direction.

Before the detailed presentation of the fluctuation modes, it is appropriate to briefly discuss their nature. For homogeneous phases the fluctuation modes are simply plane waves. On the other hand, for an ordered phase, the fluctuation modes are complex and can be written as linear combinations of Bloch waves. We define the eigenvectors of $\mathbf{C}^{\mathrm{RPA}}$ by

$$\varphi^i(\mathbf{k}) = (\varphi^i_1(\mathbf{k}), \varphi^i_2(\mathbf{k}), ..., \varphi^i_N(\mathbf{k})) \tag{28}$$

with $1 \le i \le N$. The eigenmodes are therefore indexed by the reduced wave vector, $\mathbf{k}$, and the band label, n. The effect of these fluctuation modes can be revealed in Fourier space through the scattering functions, or in real space through the structure of the interfaces between the A-rich and the B-rich domains. In real space, the effect of the least stable or most unstable mode can be obtained by perturbing the mean-field solution with the corresponding eigenfunction. The perturbed density profile of the A-blocks can be written as

$$\phi_{\mathrm{A}}(\mathbf{r}) = \phi^{(0)}_{\mathrm{A}}(\mathbf{r}) + a\sum_n \varphi^1_n(\mathbf{k})\, \psi^{\mathrm{A}}_{n\mathbf{k}}(\mathbf{r}) \tag{29}$$

where a is the amplitude of the eigenmode with the smallest eigenvalue (indicated with the superscript 1). Depending on whether the ordered phase is stable or unstable, this mode is termed the least stable or most unstable eigenmode. The contour plot defined by $\phi_{\mathrm{A}}(\mathbf{r}) = 0.5$ defines the interfaces in the melt, and the effect of the leading fluctuating mode can be observed by tuning a.

A. Scattering Functions and Fluctuation Modes of the Lamellar Phase. The scattering functions of the lamellar phase prior to its spinodal line (at $\chi Z = 10.8$, $f = 0.462$) is shown in Figure 4 for the planes $q_x = 0$ and $q_z = 0$ (the lamellar planes are parallel to the $x-y$ plane). At this point of the phase diagram, the lamellar phase is in fact metastable, and the equilibrium stable phase is cylindrical. In agreement with previous work,[17] the scattering function has two strong Bragg peaks at ($q_z = \pm k_0$, $q_x = 0$), where $k_0 = 2\pi/D$ and D is the lamellar periodicity, and two higher order Bragg peaks located at ($q_z = \pm 2k_0$, $q_x = 0$). These strong peaks signal the relatively strong lamellar ordering. We also observed four additional peaks at ($q_z = \pm k_0/2$, $q_x \approx \pm\sqrt{3}k_0/2$). As has been shown before[17] and will be demonstrated below, these four peaks correspond to in-plane fluctuations with hexagonal ordering. The calculated scattering function in the q_x-q_z plane is in good agreement with the experimentally observed one.[5] In particular, the main experimental features corresponding to the appearance of the four weak peaks due to the in-plane fluctuations, their hexagonal ordering, and the 10% difference in q_z and q_x are reproduced by the theory. A real space representation of the least-stable fluctuation mode is given in Figure 5, where the interfaces between the A-rich and the B-rich microdomains are shown for the density profiles corresponding to different a values (see eq 29). These fluctuation modes lead to undulations of the lamellae in a such a way that the minority-rich domains pinch and bulge for small values of a. For larger values of a, the minority lamellae break up to form elongated cylinders with their principal axes arranged in a hexagonal lattice with the same periodicity as that of the equilibrium cylindrical phase at this

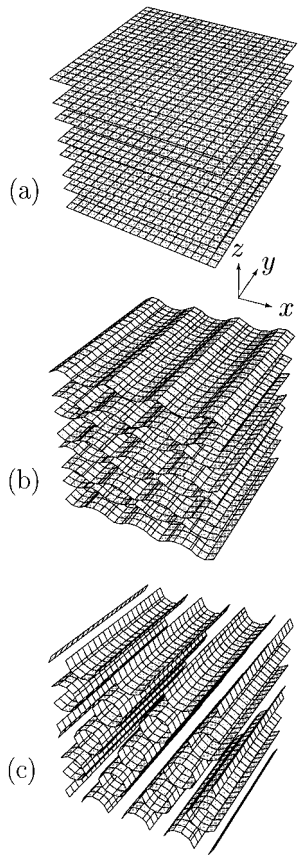

Figure 5. Three-dimensional contour plots of the lamellar phase showing the effects of the least stable mode on the lamellae at $\chi Z = 10.8$, $f = 0.462$ (shown by the symbol ○ in Figure 3). The contour plots are defined by $\phi_{\mathrm{A}}(\mathbf{r}) = \phi^{(0)}_{\mathrm{A}}(\mathbf{r}) + a\sum_n \phi^{(1)}(\mathbf{k})\, \psi^{\mathrm{A}}_{n\mathbf{k}}(\mathbf{r}) = 0.5$, where a is the amplitude of the least-stable fluctuation mode: (a) $a = 0$; (b) $a = 0.05$; (c) $a = 0.15$. Notice that, for a relatively large amplitude, the fluctuation mode leads to hexagonally-packed cylinders whose axes are parallel to the lamellae.

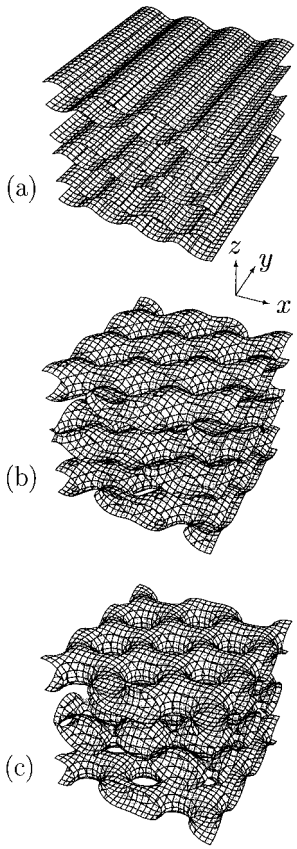

Figure 6. Three-dimensional contour plots of the lamellar phase showing the effect of the degeneracy of the least-stable modes, with $a = 0.05$, at $\chi Z = 10.8$, $f = 0.462$ (shown by the symbol ○ in Figure 3): (a) selection of a single direction for the fluctuation mode (as in Figure 4); (b) simultaneous selection of two directions for the fluctuation mode; (c) simultaneous selection of three directions of the fluctuation mode. We emphasize that this figure shows a very special case in which the three selected directions are threefold symmetric. Notice that the selection of more than one mode leads to a modulated-layered structure, reminiscent of the experimentally observed hexagonally perforated lamellar phase.

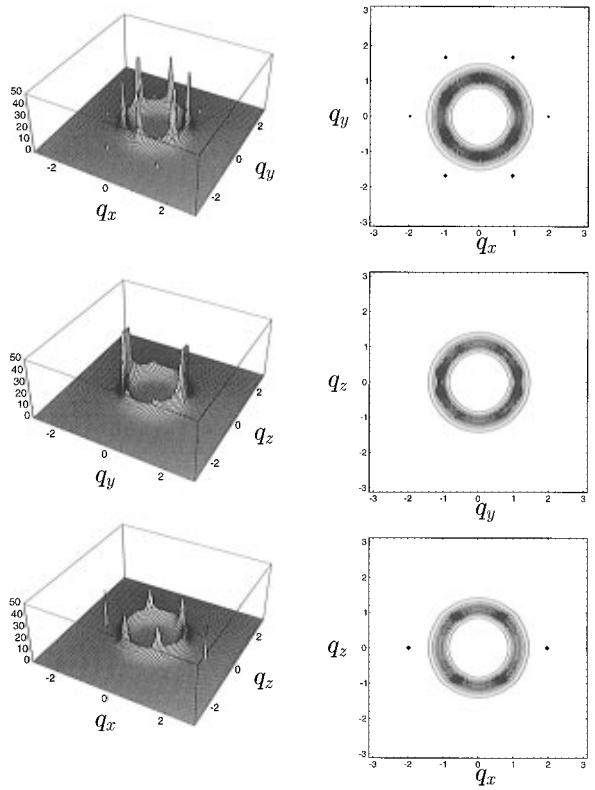

Figure 7. Scattering function of the cylindrical phase at $\chi Z = 10.9$, $f = 0.43$ prior to the outer spinodal line of this phase (shown by the symbol △ in Figure 3). The three cuts corresponding to the q_x-q_y, q_y-q_z, and q_x-q_z planes are shown in the top, middle, and bottom graphs.

point of the phase diagram. Therefore, this observation indicates that these fluctuation modes are responsible for driving the lamellar phase to the cylindrical phase with the cylinders oriented parallel to the lamellae. The epitaxial relation between the lamellar and the cylindrical structures which emerges from the theory is in agreement with the recent time-dependent Ginzburg–Landau simulation of Qi and Wang[21] and experiments.[8]

We now discuss the nature of the in-plane fluctuation modes in the lamellar phase. Because the mean-field profile is isotropic in the $x-y$ plane, the scattering function is also isotropic in the q_x-q_y plane as shown by the ring structure in Figure 4. Therefore the fluctuation modes of the lamellar phase are infinitely degenerate in the $x-y$ plane. If only one direction in the q_x-q_y plane is selected, as in Figure 5, this fluctuation mode leads to the formation of cylinders. In a real situation, however, it is most likely that many directions will be simultaneously selected. Figure 6 shows that when more than one direction is selected, the fluctuating modes lead to a modulated layered structure. Since the equilibrium state corresponds to a cylindrical phase, this modulated layered structure will eventually evolve into cylinders. However, due to the convoluted structure of the modulated layers, the transformation from this state to the cylindrical structure will involve the transport of a large amount of material. Consequently, the kinetics of this process is expected to be very slow. It is therefore plausible that when the lamellar phase becomes unstable, the polymer melt will be trapped into an intermediate modulated layered state which might be identified as an equilibrium phase in an experiment. This scenario is in agreement with the recent experiment of Hajduk *et al.*[11] which shows that the modulated layered structure is a kinetically trapped state. Likewise, in the recent work of Qi and Wang,[21] the modulated layered state is also found to be a kinetically trapped state. It should be noted that the origin of the intermediate state is the convoluted perforated layered structure. For the case of the lamellar phase, this convoluted structure is a consequence of the infinitely degenerate fluctuation modes. However, it is possible to have a convoluted structure without infinite degeneracy, as will be shown later for the spherical phase.

B. Scattering Functions and Fluctuation Modes of the Cylindrical Phase. Due to the two-dimensional nature of the cylindrical phase, the scattering function is more complex than that for the lamellar case. In order to be specific, we define the z-axis along the cylinders, the y-axis along the [01] direction of the hexagonal lattice, and the x-axis perpendicular to the y-axis. We choose to plot the scattering functions in the form of three perpendicular cuts in **q**-space corresponding to the planes defined by $q_z = 0$, $q_y = 0$, and $q_x = 0$. Because the cylindrical phase has inner and outer spinodal lines, we present the results on the scattering functions and fluctuation modes of this phase close to these two spinodal lines. Figures 7 and 8 show the scattering functions of the cylindrical phase prior to its outer and inner spinodal lines at ($\chi Z = 10.9$, $f = 0.43$) and ($\chi Z = 10.9$, $f = 0.476$), respectively. The generic features of the cylindrical scattering functions are described by the three following observations: (1) In the $q_z = 0$ plane, there are six strong hexagonally arranged

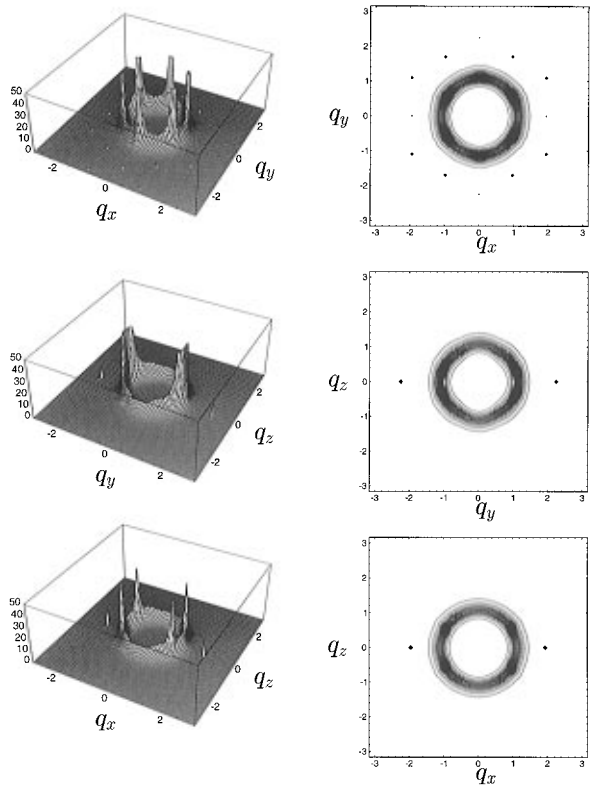

Figure 8. Scattering function of the cylindrical phase at $\chi Z = 10.9$, $f = 0.476$ prior to the inner spinodal line of this phase (shown by the symbol ▽ in Figure 3). The three cuts shown are the same as those in Figure 8.

Bragg peaks, corresponding to the hexagonal ordering of the cylinders. The six weaker secondary Bragg peaks are also visible. (2) In the $q_x = 0$ plane, there are two strong Bragg peaks located at $q_z = 0$, $q_y = \pm 2k_0/\sqrt{3}$, where $k_0 = 2\pi/D$ and D is the periodicity of the hexagonal lattice. These two peaks indicate the layered ordering of the cylindrical structure along the y-axis. (3) In the $q_y = 0$ plane, there are two weak secondary Bragg peaks located at $q_z = 0$, $q_x = \pm 2k_0$. The least-stable fluctuation modes correspond to four weak scattering peaks which are observed in the $q_x = 0$ and $q_y = 0$ planes. The exact locations of fluctuation peaks depend on the values of χZ and f, implying that the least-stable fluctuation mode near the inner spinodal line must be different from that near the outer spinodal line.

Near the outer spinodal line ($\chi Z = 10.9$, $f = 0.43$), the four fluctuation peaks are located at $q_x \approx \pm k_0/\sqrt{3}$, $q_z \approx \pm 2\sqrt{2}k_0/3$. A real space representation of these fluctuation modes is given in Figure 9 for different values of a. For small values of a, the fluctuation modes lead to the bulging and pinching of the cylinders. Larger values of a lead to a breakup of the cylinders to form spheres which are centered on a body-centered-cubic lattice with a periodicity which is identical to that of the equilibrium spherical phase at this point of the phase diagram. An epitaxial relation between the cylindrical and spherical phases therefore emerges naturally from the fluctuation modes. The cylinders are oriented along the [111] direction of the bcc lattice. The fluctuation peaks of the cylindrical phase, together with the six primary Bragg peaks in the $q_x - q_y$ plane, correspond to the 12 primary Bragg peaks of the body-centered-cubic lattice.

Close to the inner spinodal line of the cylindrical phase (at $\chi Z = 10.9$, $f = 0.476$), the scattering function

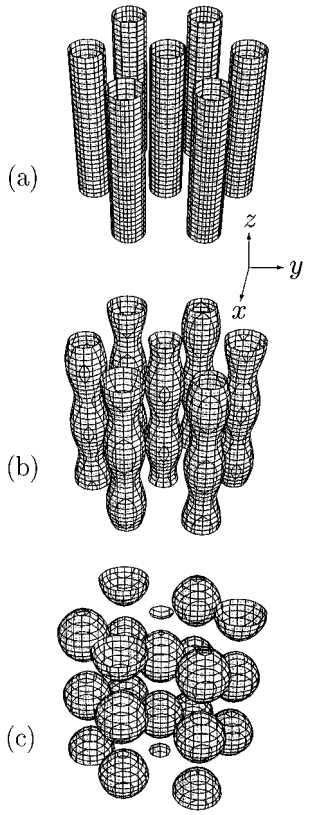

Figure 9. Three-dimensional contour plots of the hexagonal phase, at $\chi Z = 10.9$, $f = 0.43$ (shown by the symbol △ in Figure 3), showing the effects of the least-stable mode on the ordered cylinders. The contour plots have the same definition as in Figure 5: (a) $a = 0$, *i.e.* the mean-field solution; (b) $a = 0.02$; (c) $a = 0.075$. Notice that the effect of a relatively large amplitude leads to the formation of spheres which are arranged in a body-centered-cubic lattice. The [111] direction of the cubic unit cell of this lattice is along the cylindrical axis.

in the $q_y - q_z$ plane exhibits extended wings close to the two Bragg peaks. A real space representation of these fluctuation modes is given in Figure 10 for different values of a. In particular, we notice that, for small values of a, the fluctuation modes lead to a flattening of the cylinders along the [01] direction. For larger values of a, these ellipsoidal cylinders merge to form modulated layers, with a periodicity which is identical to that of the equilibrium lamellar phase at this point of the phase diagram. The epitaxial relation between the lamellar and the cylindrical phases, emerging from the least-stable eigenmode of the cylindrical phase is identical to the one we obtained from the least-stable modes of the lamellar phase.

Because the least-stable fluctuation modes of the cylindrical phase are only threefold degenerate, we expect that the kinetics of the cylindrical−lamellar and cylindrical−spherical transitions proceed directly without an intermediate state. The absence of an intermediate state in the kinetics of the cylindrical-to-spherical transition has also been found in a recent numerical study by Qi and Wang.[21] The absence of an intermediate state during the cylindrical-to-lamellar transition has been reported in the experiments of Sakurai *et al.*[9,10] In the previous subsection, we found that the lamellar-to-cylindrical transition proceeds through a long-lived intermediate modulated-layered state. Our results therefore imply that the lamellar-to-cylindrical and cylindrical-to-lamellar transitions are not reversible in their kinetic pathways.

C. Scattering Functions and Fluctuation Modes of the Spherical Phase. For the spherical phase, we

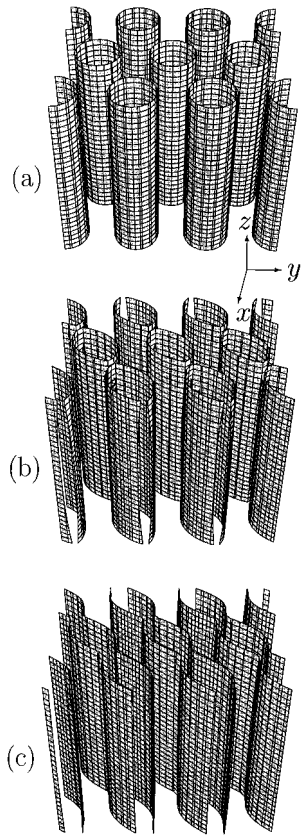

Figure 10. Three-dimensional contour plots of the hexagonal phase, at $\chi Z = 10.9$, $f = 0.476$ (shown by the symbol ∇ in Figure 3), showing the effects of the least-stable mode on the ordered cylinders: (a) $a = 0$, *i.e.* the mean-field solution; (b) $a = 0.06$; (c) $a = 0.08$. Notice that the effect of a relatively large amplitude leads to the formation of modulated lamellae parallel to the cylinders axes.

use the standard cubic unit cell to describe its geometry. We choose to plot the scattering function along three cuts in **q**-space: (i) the plane defined by $q_z = 0$ corresponding to the scattering from the (001) planes; (ii) the plane defined by $q_x + q_y + q_z = 0$ corresponding to scattering from the (111) planes; (iii) the plane defined by $q_x = q_y$ corresponding to the scattering from the (110) planes. The scattering function of the spherical phase close to its inner spinodal line at ($\chi Z = 10.8$, $f = 0.448$) is shown in Figure 11. The scattering function in the $q_z = 0$ plane shows four strong Bragg peaks and several higher-order Bragg peaks signaling the fourfold symmetry of this phase along the [100] (or equivalent) direction. On the other hand, the scattering function exhibits six strong Bragg peaks in the plane defined by $q_x + q_y + q_z = 0$. These strong peaks signal the threefold symmetry of the spherical structure in the [111] direction. In the plane defined by $q_x = q_y$, there are two strong Bragg peaks corresponding to the twofold symmetry along the [110] directions. The least-stable fluctuation modes of the spherical phase close to its spinodal line are manifested by the four wings in the plane $q_x = q_y$. A real space representation of these fluctuation modes is shown in Figure 12 for three different values of a. For small values of a, the fluctuation modes lead to the flattening of the spheres along the [110] direction. Increasing a leads to the merging of these distorted spheres, resulting in a perforated layered structure perpendicular to the [110] direction. Since the equilibrium phase at this point of the phase diagram corresponds to the cylindrical phase, this convoluted structure will appear as an intermediate state during the kinetics of the transition from the

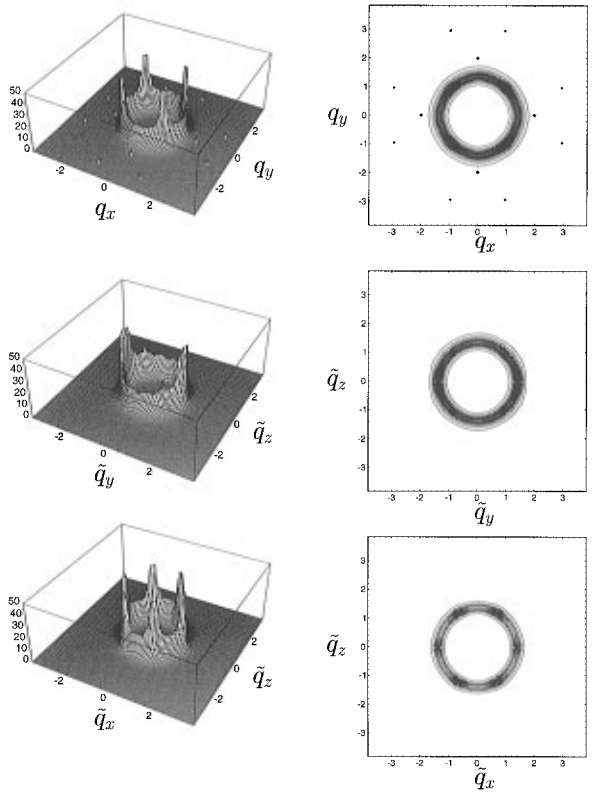

Figure 11. Scattering function of the spherical phase at $\chi Z = 10.8$, $f = 0.448$ prior to the inner spinodal line of this phase (shown by the symbol □ in Figure 3). The top graphs of this figure correspond to the cut along the $q_x - q_y$ plane. The middle graphs correspond to a cut along the plane defined by $q_x + q_y + q_z = 0$; $\tilde{q}_x$ and $\tilde{q}_y$ are defined by $\tilde{q}_x = (q_y - q_x)/\sqrt{2}$ and $\tilde{q}_y = (q_x + q_y - 2q_z)/\sqrt{6}$. The bottom graph corresponds to a cut along the plane defined by $q_x = q_y$; $\tilde{q}_x$ is defined by $\tilde{q}_x = \sqrt{2}q_x$.

spherical to the cylindrical phase. Therefore, the identification of the least-stable modes of the spherical phase close to its inner spinodal lines leads to the conclusion that the cylindrical−spherical and the spherical−cylindrical transitions are not reversible. We found that whereas the cylindrical−spherical transition proceeds directly, the spherical−cylindrical transition proceeds through an intermediate modulated layered state. To our best knowledge, experimental studies of the kinetics of the spherical−cylindrical transition are not yet available.

V. Scattering Functions of the HPL Phase

From the stability analysis, the HPL phase is metastable in the middle of the lamellar phase. We have argued in section IV that the experimentally observed modulated layered phases are long-lived intermediate structures as a consequence of the infinite degeneracy of the least-stable fluctuation modes of the lamellar phase. Despite the instability of the HPL phase in most of the phase diagram, we present in this section the calculated scattering functions of this phase for completeness. We choose the coordinate system in such a way that the z-axis is perpendicular to the layers. It should be noted that, due to the hexagonal symmetry of this phase, the two in-plane directions along the x-axis and the y-axis are not equivalent. The scattering function of the HPL phase, prior to its spinodal line (at $\chi Z = 10.8$, $f = 0.476$), is plotted in Figure 13 for the three cuts defined by $q_z = 0$, $q_x = 0$, and $q_y = 0$. The threefold symmetry of the perforated structure is evident in the scattering function in the $q_z = 0$ plane. We

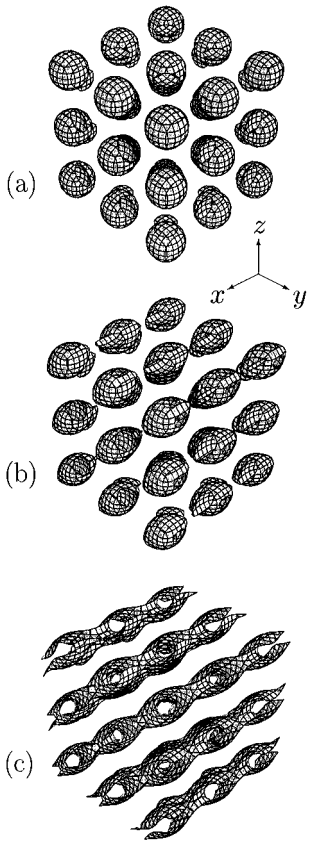

Figure 12. Three-dimensional contour plots of the spherical phase, at $\chi Z = 10.8$, $f = 0.448$ (shown by the symbol □ in Figure 3), showing the effects of the most unstable mode on the ordered phase. The view is along the [110] direction: (a) $a = 0$, *i.e.* the mean-field solution; (b) $a = 0.025$; (c) $a = 0.05$. Notice that the effect of the least-stable fluctuation mode leads to a layered structure perpendicular to the [110] direction.

should notice that these are not Bragg peaks. Six weak secondary peaks are clear in this plane. The stacking of the holes is revealed by the four strong Bragg peaks in the scattering function in the $q_x = 0$ plane. The lamellar ordering of the system is best reflected in the two strong Bragg peaks in the scattering function in the $q_y = 0$ plane. The least-stable modes correspond to the four weak scattering peaks in the $q_y = 0$ plane. It is of interest to make the comparison between the calculated scattering function of the HPL phase and the corresponding experiments. Experimentally, for shear oriented samples located in the phase diagram at the lamellar−cylindrical phase boundary,[5,25] the measured scattering functions, presumably from the HML/HPL structures, show sixfold symmetric scattering peaks in the $q_z = 0$ plane. For the directions parallel to the layers, two strong Bragg peaks and four satellite peaks are observed. These two features are indeed present in our calculated scattering functions for the HPL phase in the $q_z = 0$ and $q_y = 0$ planes. Therefore it is rather difficult to distinguish, on the basis of the scattering functions alone, between the experimentally observed HML/HPL phases and the model HPL phase with the space group $R\bar{3}m$, which we have used in our calculation. Nevertheless, we notice that the measurement of the scattering functions on the third plane[25] is different from the calculated one on the plane $q_x = 0$. This suggests that the observed HML/HPL structure does not correspond to the space group $R\bar{3}m$. A real space representation of the most unstable mode in the HPL phase is given in Figure 14.

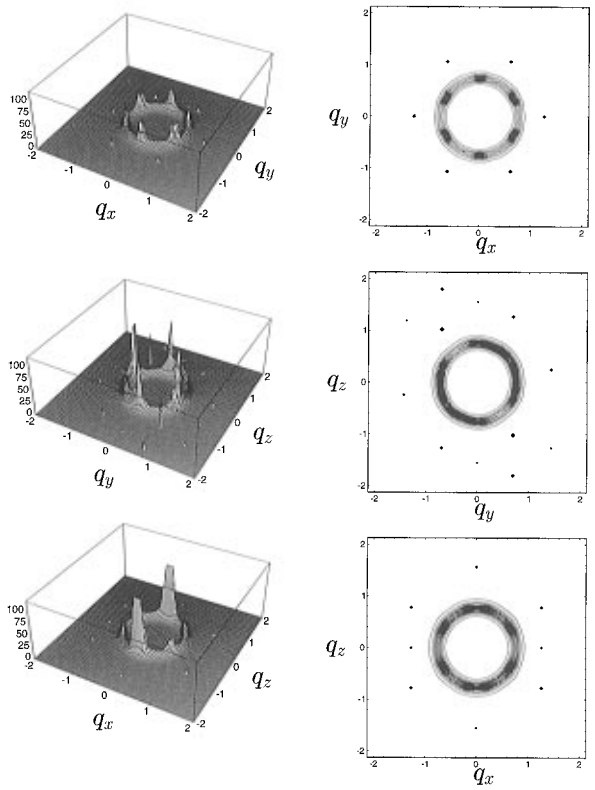

Figure 13. Scattering function of the hexagonally-perforated lamellar phase at $\chi Z = 10.8$, $f = 0.476$, prior to the spinodal line of this phase (shown by the symbol + in Figure 3). The top graphs of this figure correspond to the q_x−q_y plane, the middle graphs correspond to the q_y−q_z plane, and the bottom graphs correspond to the q_x−q_z plane.

VI. Double-Gyroid Phase

In this work we focused on the weak segregation region of the phase diagram, where self-consistent mean-field theory predicts that the double-gyroid phase is not an equilibrium phase for $\chi Z < 11.14$. In this section we present results on the stability of this structure up to $\chi Z = 12$. For this complex structure, the number of plane waves needed for the calculations increases rapidly with the degree of segregation. The following results were obtained for a limited, but large, number of plane waves (up to $N = 783$). The stability analysis along the cylindrical−lamellar phase boundary shows that surprisingly the double-gyroid structure is unstable for $\chi Z \leq 12$, although the mean-field calculation shows that this phase is stable in a narrow channel along the cylindrical−lamellar phase boundary for $\chi Z \geq 11.14$.[24] The convergence of the smallest eigenvalue λ_1 of $\mathbf{C}^{\mathrm{RPA}}$ with the number of plane waves is demonstrated in Table 1 for two points along the lamellar−cylindrical phase boundary corresponding to ($\chi Z = 10.75$, $f = 0.47$) and ($\chi Z = 12$, $f = 0.43$). It is evident from this table that λ_1 has converged for $\chi Z = 10.75$ for about 400 plane waves. On the other hand, for $\chi Z = 12$ there is still a slight variation in the value of λ_1, even up to 783 plane waves. This clearly demonstrates that the double-gyroid structure is thermodynamically unstable at $\chi Z = 10.75$. On the other hand, the results also indicate that the double-gyroid structure is unstable at ($\chi Z = 12$, $f = 0.43$), where mean-field theory predicts a stable double-gyroid phase.[24] Although we cannot exclude the possibility of not having used enough plane waves for the larger values of χZ, it is most likely that λ_1 will remain negative for larger values of N. This observation leads us to believe that the double-gyroid phase is indeed an unstable phase at this point of the

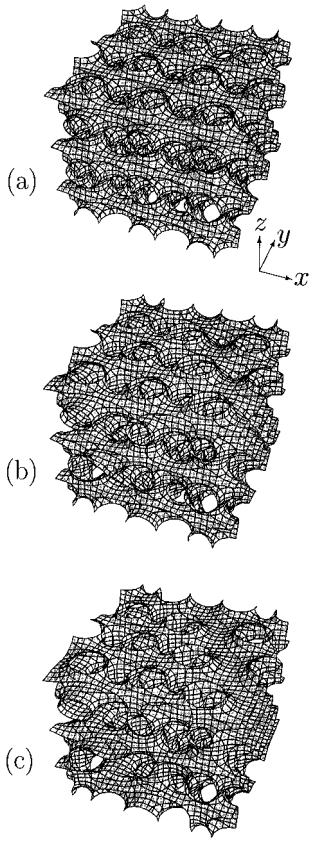

Figure 14. Three-dimensional contour plots of the HPL phase, at $\chi Z = 10.8$, $f = 0.476$ (shown by the symbol + in Figure 3), showing the effect of the most unstable fluctuation mode: (a) $a = 0$, *i.e.* the mean-field solution; (b) $a = 0.05$; (c) $a = 0.10$.

Table 1. Smallest Eigenvalue, λ_1, of C^{RPA} as a Function of the Number of Plane Waves, N, for Two Cases: (1) ($\chi Z = 10.75$, $f = 0.469$); (2) ($\chi Z = 12$, $f = 0.43$)

N	case 1	case 2
139	-0.5521×10^{-2}	-1.7778×10^{-2}
259	-0.5216×10^{-2}	-0.9891×10^{-2}
415	-0.5099×10^{-2}	-1.3447×10^{-2}
639	-0.5099×10^{-2}	-1.2999×10^{-2}
783		-1.2969×10^{-2}

phase diagram, where mean-field theory predicts a stable double-gyroid phase. Another interesting observation is that λ_1 becomes more negative as χZ is increased, suggesting that the double-gyroid phase becomes even more unstable for stronger segregation (larger χZ).

We have not calculated the scattering functions of the double-gyroid phase, since this phase is unstable. However, we have identified the most unstable fluctuation modes of this phase. In particular, we found the result that, for $\chi Z = 10.75$, $f = 0.469$, the most unstable modes drive the double-gyroid structure into modulated cylinders which are arranged in a hexagonal lattice as shown in Figure 15. These cylinders are oriented along the [111] direction of the cubic unit cell of the double-gyroid structure. The most unstable fluctuation mode leads to the epitaxial relation between the cylindrical and the double-gyroid phases, which is identical to that recently observed by Schultz *et al.*[26] This geometric relation between the two phases was also noticed from mean-field calculations.[27]

In order to put the above results in perspective, it is helpful to summarize the salient features of the experimental phase diagram as given by Bates *et al.*[2] On the basis of the recent experiment of Hajduk *et al.*,[11] the

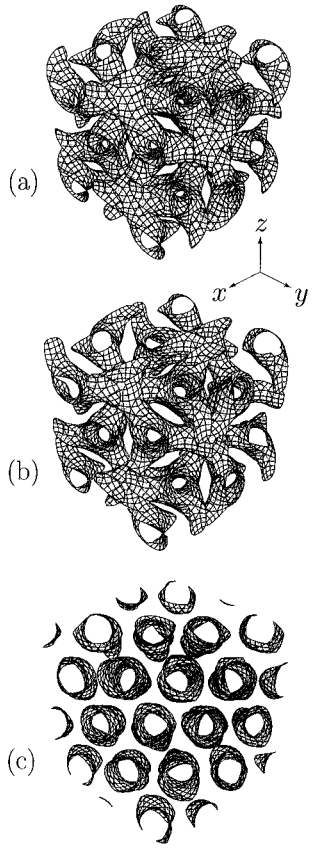

Figure 15. Three-dimensional contour plots of the double-gyroid phase, at $\chi Z = 10.75$, $f = 0.469$ (shown by the symbol $\times$ in Figure 3), showing the effect of the most unstable fluctuation mode. The view is along the [111] direction of the cubic unit cell of this structure: (a) $a = 0$, *i.e.* the mean-field solution (Notice the similarity between this structure and the several reported patterns obtained from transmission electron microscopy); (b) $a = 0.025$; (c) $a = 0.15$. Notice that the most unstable mode leads to hexagonally-packed modulated cylinders which are oriented along the [111] direction of the cubic unit cell.

time-dependent Ginzburg−Landau theory of Qi and Wang,[21] and the present theoretical study, the HML/HPL structures in the experimental phase diagrams can be attributed to intermediate states. The three classical phases are present in all diblock copolymer systems. On the other hand, the double-gyroid phase is only observed in diblock copolymers at small $\bar{Z} = (\rho_0^2 b^6/6^3)Z$ and at weak segregations.[2] This revised phase behavior strongly suggests that the double-gyroid phase is intimately associated with fluctuations. This observation correlates well with our theoretical result showing that the mean-field solution of the double-gyroid phase, corresponding to $\bar{Z} \to \infty$, is not stable. The appearance of the double-gyroid phase is therefore due to higher-order fluctuations.

VII. Conclusion

In this paper, we have presented a theory for anisotropic fluctuations in ordered phases of diblock copolymer melts. Because of the connectivity of the polymer chains and the periodicity of the ordered phases, the chain conformations are described by a modified diffusion equation which is analogous to the Schrödinger equation of an electron in a periodic potential. Exploiting the well-known Bloch's theorem, we formulated the theory in reciprocal space and determined the eigenvalues of the chain diffusion operator, from which a useful analogy to the theory of energy bands in crystal-

line solids emerged. In particular, the origin of the anisotropic fluctuations is intimately connected to the presence of eigenvalue bands similar to electronic energy bands. As the energy bands are important for the electronic properties of solids, the eigenvalue bands are crucial for calculating the elastic properties of ordered diblock copolymer melts. The theory is used to calculate the stability (spinodal) lines of the ordered phases in the weak segregation regime. We found that the lamellar, cylindrical, and spherical one-phase regions are encapsulated by their spinodal lines, revealing the robustness of these three "classical" phases which are observed in diblock copolymer melts. An important result of the theory is that the HPL phase is unstable along the lamellar−cylindrical phase boundary, where it has been identified experimentally; this layered phase is only metastable in the middle of the lamellar one-phase region.

The investigation of the least-stable eigenmodes of the various phases shows that when the lamellar phase is driven into the hexagonal phase, the kinetics of the transition proceeds through a long-lived intermediate modulated-layered state which we believe corresponds to the experimentally observed hexagonally modulated/perforated lamellar phase. This finding is in agreement with the recent experiment of Hajduk *et al.*[11] and the time-dependent Ginzburg−Landau calculations of Qi and Wang.[21] The least-stable mode of the hexagonal phase close to its inner spinodal line corresponds, on the other hand, to a lamellar phase. Therefore, the lamellar−cylindrical transition is not reversible. The analysis of the most unstable eigenmode of the cylindrical phase when it is driven into the spherical phase shows that the cylinders transform directly into a body-centered-cubic arrangement of spheres without an intermediate state. In contrast, when the spherical phase is driven into the cylindrical phase, the transformation proceeds through an intermediate state. From this we concluded that the cylindrical−spherical transition is also irreversible. The availability of the eigenmodes from the theory is exploited to calculate the scattering functions of the ordered phases.

We also analyzed the stability of the recently-identified double-gyroid phase. Surprisingly, we found that this phase is unstable around the triple point at $\chi Z = 11.14$. At stronger segregations, we found that this phase is unstable, although we do not exclude the possibility of not having used enough plane waves in our expansion (we have used up to $N = 783$). The results seem to indicate that the mean-field solution corresponds to a saddle point. The results for the double-gyroid phase are in fact in agreement with the recent experiments of Bates *et al.*[2] which find that the double-gyroid phase is only stable for polymer chains with low molecular weight and at weak segregation, leading to the speculation that this phase might be induced by fluctuations. The inclusion of higher-order composition fluctuations is possible within the theory and could be used to see if the double-gyroid phase will be stabilized. However, this is beyond the scope of the present work. The most unstable mode of the double-gyroid phase corresponds to hexagonally-packed cylinders along the [111] direction of the double-gyroid phase. The epitaxial relation between the double-gyroid phase and the cylindrical phase is in agreement with the recent experiments of Schultz *et al.*[26]

Acknowledgment. We thank Prof. C. Yeung, Dr. D. A. Hajduk, and Dr. M. W. Matsen for useful discussions. M.L. and R.C.D. acknowledge the support from the NSERC of Canada.

Appendix A: Reciprocal Space Two-Point Cumulants

In this appendix, we give the expressions of the reciprocal space forms of the two-point cumulants in our scaled units. The derivation of these cumulants can be found in ref 18.

$$C^{AA}_{n,n'}(\mathbf{k}) = \frac{f_A^2}{Q_c}\sum_{n_1}\sum_{n_2}\sum_{n_3}\sum_{n_4} \times \frac{g(\epsilon^A_{n_2\mathbf{k}} f_A - \epsilon^A_{n_1\mathbf{0}} f_A) - g(\epsilon^A_{n_3\mathbf{0}} f_A - \epsilon^A_{n_1\mathbf{0}} f_A)}{\epsilon^A_{n_3\mathbf{0}} f_A - \epsilon^A_{n_2\mathbf{k}} f_A} e^{-\epsilon^A_{n_1\mathbf{0}} f_A - \epsilon^B_{n_4\mathbf{0}} f_B} \times [\vartheta^A_{n_1} \Psi^A_{n,n_1,n_2}(\mathbf{k})\, \Psi^{A*}_{n',n_3,n_2}(\mathbf{k})\, Y^{AB}_{n_3,n_4}(\mathbf{0}) \vartheta^{B*}_{n_4} + \vartheta^{A*}_{n_1} \Psi^{A*}_{n,n_3,n_2}(\mathbf{k})\, \Psi^A_{n',n_1,n_2}(\mathbf{k})\, Y^{AB*}_{n_3,n_4}(\mathbf{0})\, \vartheta^B_{n_4}] \quad \text{(A1)}$$

$$C^{AB}_{n,n'}(\mathbf{k}) = \frac{f_A f_B}{Q_c}\sum_{n_1}\sum_{n_2}\sum_{n_3}\sum_{n_4} g(\epsilon^A_{n_2\mathbf{k}} f_A - \epsilon^A_{n_1\mathbf{0}} f_A) g(\epsilon^B_{n_3\mathbf{k}} f_B - \epsilon^B_{n_4\mathbf{0}} f_B) e^{-\epsilon^A_{n_1\mathbf{0}} f_A - \epsilon^B_{n_4\mathbf{0}} f_B} \vartheta^A_{n_1} \Psi^A_{n,n_1,n_2}(\mathbf{k})\, Y^{AB}_{n_2,n_3}(\mathbf{k}) \times \Psi^{B*}_{n',n_4,n_3}(\mathbf{k})\, \vartheta^{B*}_{n4} \quad \text{(A2)}$$

$$C^{BA}_{n,n'}(\mathbf{k}) = \frac{f_A f_B}{Q_c}\sum_{n_1}\sum_{n_2}\sum_{n_3}\sum_{n_4} g(\epsilon^B_{n_2\mathbf{k}} f_B - \epsilon^B_{n_1\mathbf{0}} f_B) g(\epsilon^A_{n_3\mathbf{k}} f_A - \epsilon^A_{n_4\mathbf{0}} f_A) e^{-\epsilon^A_{n_4\mathbf{0}} f_A - \epsilon^B_{n_1\mathbf{0}} f_B} \vartheta^B_{n_1} \Psi^B_{n,n_1,n_2}(\mathbf{k})\, Y^{BA}_{n_2,n_3}(\mathbf{k}) \times \Psi^{A*}_{n',n_4,n3}(\mathbf{k})\, \vartheta^{A*}_{n_4} \quad \text{(A3)}$$

$$C^{BB}_{n,n'}(\mathbf{k}) = \frac{f_B^2}{Q_c}\sum_{n_1}\sum_{n_2}\sum_{n_3}\sum_{n_4} \times \frac{g(\epsilon^B_{n_2\mathbf{k}} f_B - \epsilon^B_{n_1\mathbf{0}} f_B) - g(\epsilon^B_{n_3\mathbf{0}} f_B - \epsilon^B_{n_1\mathbf{0}} f_B)}{\epsilon^B_{n_3\mathbf{0}} f_B - \epsilon^B_{n_2\mathbf{k}} f_B} e^{-\epsilon^B_{n_1\mathbf{0}} f_B - \epsilon^A_{n_4\mathbf{0}} f_A} \times [\vartheta^B_{n_1} \Psi^B_{n,n_1,n_2}(\mathbf{k})\, \Psi^{B*}_{n',n_3,n_2}(\mathbf{k})\, Y^{BA}_{n_3,n_4}(\mathbf{0})\, \vartheta^{A*}_{n_4} + \vartheta^{B*}_{n_1} \Psi^{B*}_{n,n_3,n_2}(\mathbf{k})\, \Psi^B_{n',n_1,n_2}(\mathbf{k})\, Y^{BA*}_{n_3,n_4}(\mathbf{0})\, \vartheta^A_{n_4}] \quad \text{(A4)}$$

where the various functions in the equations above are defined by

$$g(x) = \frac{1 - e^{-x}}{x} \quad \text{(A5)}$$

$$\vartheta^\alpha_n = \sqrt{V} u^\alpha_{n0}(0) \quad \text{(A6)}$$

$$Y^{\alpha\beta}{}_{n,n'}(\mathbf{k}) = \sum_{\mathbf{G}} u^{\alpha*}_{n\mathbf{k}}(\mathbf{G})\, u^\beta_{n'\mathbf{k}}(\mathbf{G}) \quad \text{(A7)}$$

$$\Psi^\alpha_{n1,n2,n3}(\mathbf{k}) = \frac{1}{\sqrt{V}}\sum_{\mathbf{G}_1}\sum_{\mathbf{G}_2} u^{A*}_{n_1\mathbf{k}}(\mathbf{G}_1)\, u^{\alpha*}_{n_20}(\mathbf{G}_2) u^\alpha_{n_3\mathbf{k}}(\mathbf{G}_1+\mathbf{G}_2) \quad \text{(A8)}$$

Appendix B: Computational Methods for Reciprocal Space

The study of anisotropic fluctuations starts with the identification of the space groups for the ordered phases. The ordered diblock copolymer phases considered in this

work are the one-dimensional lamellar phase, the hexagonal phase with space group $p6m$, the BCC phase with space group $Im3m$, the double-gyroid phase with space group $Ia\bar{3}d$, and the HML/HPL phase with space group $R\bar{3}m$. For a given ordered phase, the reciprocal lattice vectors $\mathbf{G}^n$ are identified. These reciprocal lattice vectors are ordered according to their magnitudes $|\mathbf{G}^n|^2 = \lambda_n$, starting with $|\mathbf{G}^1|^2 = 0$, $0 = \lambda_1 < \lambda_2 \leq \lambda_3 \leq ....$ The plane waves corresponding to these reciprocal lattice vectors, $\exp(i\mathbf{G}^n\cdot\mathbf{r})$, are used as the basis functions for the eigenproblem defined by eq 21. For the computations, the number of the reciprocal lattice vectors N is limited to large N. The $N \times N$ eigenproblem for the polymer chains (eq 21) is then solved using standard software packages.

For the calculation of the anisotropic correlation functions, it is necessary to obtain an exact mean-field solution for the ordered phase. For the mean-field solutions, further simplification of the basis functions can be made on the basis of the observation that the fields $\phi_\alpha^{(0)}(\mathbf{r})$ and $\omega_\alpha^{(0)}(\mathbf{r})$ and the end-integrated propagators, $q_\alpha^{(\dagger)}(\mathbf{r})$, are periodic functions. The symmetry of the ordered structure ensures that the Fourier coefficients of these periodic functions for the reciprocal lattice vectors within one star are related.[28] A set of new basis functions can be defined using this observation. Each function is a linear combination of plane waves with wave vectors $\mathbf{G}_i^n$ satisfying the condition $|\mathbf{G}_i^n|^2 = \lambda_n$:

$$f_n(\mathbf{r}) = \frac{1}{\sqrt{N_n}} \sum_{i\in n} e^{i\mathbf{G}_i^n\cdot\mathbf{r}} S_i^n \tag{B1}$$

where S_i^n assumes the values ± 1 according to the space group specifications and N_n is the total number of reciprocal lattice vectors belonging to the star n. The values of N_n and S_i^n can be found from the *International Table of Crystallography*.[28] This set of basis functions is used in the mean-field theory of diblock copolymers.[24]

Within mean-field theory it is convenient to define the end-integrated propagators

$$q_\alpha(\mathbf{r},t) = \int d\mathbf{r}_1\, Q_\alpha^{(0)}(\mathbf{r},t|\mathbf{r}_1) \tag{B2}$$

$$q_\alpha^\dagger(\mathbf{r},t) = \int d\mathbf{r}_1\, d\mathbf{r}_2\, Q_\alpha^{(0)}(\mathbf{r},t|\mathbf{r}_1)\, Q_\beta^{(0)}(\mathbf{r}_1,f_\beta|\mathbf{r}_2) \tag{B3}$$

It can be shown that the two propagators above satisfy the diffusion equations

$$\frac{\partial}{\partial t} q_\alpha(\mathbf{r},t) = \nabla^2 q_\alpha(\mathbf{r},t) - \omega_\alpha(\mathbf{r})\, q_\alpha(\mathbf{r},t) \tag{B4}$$

$$\frac{\partial}{\partial t} q_\alpha^\dagger(\mathbf{r},t) = \nabla^2 q_\alpha^\dagger(\mathbf{r},t) - \omega_\alpha(\mathbf{r}) q_\alpha^\dagger(\mathbf{r},t) \tag{B5}$$

with the boundary conditions $q_\alpha(\mathbf{r},0) = 1$ and $q_\alpha^\dagger(\mathbf{r},0) = q_\beta(\mathbf{r},f_\beta)$. If one expands the propagators in terms of the basis functions $f_n(\mathbf{r})$, the components of the end-integrated propagators satisfy the differential equations

$$\frac{dq_{\alpha,n}(t)}{dt} = -\sum_m A_{nm}^\alpha q_{\alpha,m}(t) \tag{B6}$$

$$\frac{dq_{\alpha,n}^\dagger(t)}{dt} = -\sum_m A_{nm}^\alpha q_{\alpha,m}^\dagger(t) \tag{B7}$$

where the matrix elements of $\mathbf{A}^\alpha$ are given by

$$A_{nm}^\alpha = -\frac{\lambda_n}{D^2}\delta_{nm} - \sum_l \Gamma_{nml}\omega_{\alpha,l} \tag{B8}$$

and the coefficients Γ_{nml} are defined by

$$\Gamma_{nml} = \frac{1}{\sqrt{N_n N_m N_l}} \sum_{i\in n}\sum_{j\in m}\sum_{k\in l} \delta_{\mathbf{G}_i^n+\mathbf{G}_j^m,\mathbf{G}_k^l} S_i^n S_j^m S_k^l \tag{B9}$$

Because $\mathbf{A}^\alpha$ is Hermitian, its normalized eigenvectors, $\{\Phi_\alpha^{(n)}\}$, form a complete orthonormal basis, and their corresponding eigenvalues $\{\xi_\alpha^{(n)}\}$ are real. The coefficients $q_{\alpha,i}(t)$ and $q_{\alpha,i}^\dagger(t)$ can be expanded as a linear combination of the eigenvectors of $\boldsymbol{A}^\alpha$,

$$q_{\alpha,i}(t) = \sum_n q_\alpha^{(n)}(t)\Phi_{\alpha,i}^{(n)} \tag{B10}$$

$$q_{\alpha,i}^\dagger(t) = \sum_n q_\alpha^{\dagger(n)}(t)\Phi_{\alpha,i}^{(n)} \tag{B11}$$

The problem therefore reduces to finding the coefficients $q_\alpha^{(m)}(t)$ and $q_\alpha^{\dagger(m)}(t)$. Equations B6 and B7 combined with the boundary conditions lead to

$$q_{\alpha,i}(t) = \sum_n \Phi_{\alpha,1}^{(n)}\Phi_{\alpha,i}^{(n)} e^{-\xi_\alpha^{(n)}t} \tag{B12}$$

$$q_{\alpha,i}^\dagger(t) = \sum_n q_\alpha^{\dagger(n)}(0)\Phi_{\alpha,i}^{(n)} e^{-\xi_\alpha^{(n)}t} \tag{B13}$$

where $q_\alpha^{\dagger(n)}(0)$ is determined from the inital condition

$$q_\alpha^{\dagger(n)}(0) = \sum_m \Phi_{\beta,1}^{(m)} e^{-\xi_\beta^{(m)}f_\beta} \sum_i \Phi_{\beta,i}^{(m)}\Phi_{\alpha,i}^{(n)} \tag{B14}$$

From the self-consistent mean-field equation (eq 9), an expression for the components of the volume fractions is obtained

$$\phi_{\alpha,l} = \frac{1}{q_{\alpha,1}^\dagger(f_\alpha)} \sum_n\sum_m \Gamma_{nml} \sum_p\sum_q \Phi_{\alpha,1}^{(p)}\Phi_{\alpha,n}^{(p)}\Phi_{\alpha,m}^{(q)} q_\alpha^{\dagger(q)}(0) \times \frac{1 - e^{-f_\alpha(\xi_\alpha^{(p)}+\xi_\alpha^{(q)})}}{\xi_\alpha^{(p)} + \xi_\alpha^{(q)}} \tag{B15}$$

and the single-chain partition function is given by $Q_c = q_{A,1}^\dagger(f) = q_{B,1}^\dagger(1-f)$.

Since the free energy of the system is invariant under a constant shift in the auxiliary fields, we will further use the convention $\int d\mathbf{r}\, \omega_\alpha(\mathbf{r}) = 0$, leading to $\omega_{\alpha,1} = \eta_1 = 0$. Thus the self-consistent equations eq 8) become

$$\begin{aligned} \omega_{A,i} &= \chi Z(\phi_{B,i} - f_B\delta_{i,1}) + \eta_i \\ \omega_{B,i} &= \chi Z(\phi_{A,i} - f_A\delta_{i,1}) + \eta_i \end{aligned} \tag{B16}$$

with $\phi_{\alpha,1} = f_\alpha$. The mean-field free energy per chain less that of the homogeneous phase is given by

$$\Delta F^{(0)} = \chi Z \sum_n \phi_{A,n}^2 - \ln\, q_{A,1}^\dagger(f_A) \tag{B17}$$

The reciprocal space self-consistent mean-field method for a broken symmetry phase in a diblock copolymer system is implemented numerically as follows:

(1) At a certain point of the phase diagram parameter space (χZ,f) and for a given phase with a specified space group, determine the reciprocal vectors $\{\mathbf{G}_i^n\}$ and the coefficient $\{S_n\}$[28] and calculate the coefficients Γ_{nml} using eq B9.

(2) Choose a lattice periodicity D.

(3) Make an initial guess for $\phi_{\alpha,i}$ and calculate the initial values of $\omega_{\alpha,i}$ using eq B16 and assuming $\eta_i = 0$.

(4) Compute the matrix elements A_{nm}^{α} and solve the eigenvalue problem $\mathbf{A}^{\alpha}\Phi_{\alpha}^{(n)} = \zeta_{\alpha}^{(n)}\Phi_{\alpha}^{(n)}$. Then calculate the volume fractions using eq B15.

(5) Using eqs B16, calculate the Lagrange multiplier η_i as $\eta_i = (\omega_{A,i} + \omega_{B,i})/2$, and then calculate

$$\delta\omega_{A,i} = \chi Z\phi_{B,i} + \eta_i - \omega_{A,i} \tag{B18}$$

$$\delta\omega_{B,i} = \chi Z\phi_{A,i} + \eta_i - \omega_{B,i} \tag{B19}$$

$$\delta\phi_i = \delta\phi_{A,i} + \delta\phi_{B,i} \tag{B20}$$

If the values of $\delta\phi_i$, $\delta\omega_{A,i}$, and $\delta\omega_{B,i}$ are smaller than a certain convergence criterion (*e.g.* 10^{-6}), proceed to step 6. Otherwise, calculate new values of $\omega_{\alpha,i}$ using

$$\omega'_{\alpha,i} = \omega_{\alpha,i} + \gamma\delta\omega_{\alpha,i} - \beta\delta\phi_i \tag{B21}$$

where γ and β are small positive numbers (we used $\beta = \gamma = 0.1$), and return to step 2.

(6) Compute the free energy density using eq B14.

The procedure is then repeated for a different lattice periodicity, D, until the lowest free energy density is obtained.

References and Notes

(1) Bates, F. S.; Fredrickson, G. H. *Annu. Rev. Phys. Chem.* **1990**, *41*, 525.
(2) Bates, F. S.; Schulz, M. F.; Khandpur, A. K.; Förster, S. F.; Rosedale, J. H. *Faraday Discuss.* **1994**, *98*, 7.
(3) Seul, M.; Andelman, D. *Science* **1995**, *267*, 476.
(4) Leibler, L. *Macromolecules* **1980**, *13*, 1602.
(5) Hamley, I. W.; Koppi, K. A.; Rosedale, J. H.; Bates, F. S.; Almdal, K.; Mortensen, K. *Macromolecules* **1993**, *26*, 5959.
(6) Hajduk, D. A.; Harper, P. E.; Gruner, S. M.; Honeker, C. C.; Kim, G.; Thomas, E. L.; Fetters, L. J. *Macromolecules* **1994**, *27*, 4063.
(7) Cohen, R. E.; Bates, F. S. *J. Polym. Sci.: Polym. Phys. Ed.* **1980**, *18*, 2143.
(8) Hajduk, D. A.; Gruner, S. M.; Rangarajan, P.; Register, R. A.; Fetters, L. J.; Honeker, C. C.; Albalak, R. J.; Thomas, E. L. *Macromolecules* **1994**, *27*, 490.
(9) Sakurai, S.; Momii, T.; Taie, K.; Shibayama, M.; Nomura, S.; Hashimoto, T. *Macromolecules* **1993**, *26*, 485.
(10) Sakurai, S.; Umeda, H.; Taie, K.; Nomura, S. *J. Chem. Phys.* **1996**, *105*, 8902.
(11) Hajduk, D. A. Private communication.
(12) Matsen, M. W.; Bates, F. S. *Macromolecules* **1996**, *29*, 1091.
(13) Fredrickson, G. H.; Helfand, E. *J. Chem. Phys.* **1987**, *87*, 697.
(14) Brasovskii, S. A. *Zh. Eksp. Teor. Fiz.* **1975**, *68*, 175 (*Sov. Phys. JETP* **1975**, *41*, 85).
(15) Mayes, A. M.; Olvera de la Cruz, M. *J. Chem. Phys.* **1991**, *95*, 1670.
(16) Muthukumar, M. *Macromolecules* **1993**, *26*, 5259.
(17) Yeung, C.; Shi, A.-C.; Noolandi, J.; Desai, R. C. *Macromol. Theory Simul.* **1996**, *5*, 291.
(18) Shi, A.-C.; Noolandi, J.; Desai, R. C. *Macromolecules* **1996**, *29*, 6487.
(19) Laradji, M.; Shi, A.-C.; Desai, R. C.; Noolandi, *J. Phys. Rev. Lett.* **1997**, *78*, 2577.
(20) Ashcroft, N. W.; Mermin, N. D. *Solid State Physics*; Saunders College: Philadelphia, PA, 1976; Chapters 8 and 9.
(21) Qi, S.; Wang, Z.-G. *Phys. Rev. Lett.* **1996**, *76*, 1679; *Phys. Rev. E* **1997**, *55*, 1682.
(22) Hong, K. M.; Noolandi, J. *Macromolecules* **1981**, *14*, 727.
(23) Doi, M.; Edwards, S. F. *The Theory of Polymer Dynamics*; Oxford University Press: London, 1986.
(24) Matsen, M. W.; Schick, M. *Phys. Rev. Lett.* **1994**, *72*, 2041.
(25) Hamley, I. W.; Gehlsen, M. D.; Khandpur, A. K.; Koppi, K. A.; Rosedale, J. H.; Schultz, M. F.; Bates, F. S.; Almdal, K.; Mortensen, K. J. *Phys. II* **1994**, *4*, 2161.
(26) Schultz, M. F.; Bates, F. S.; Almdal, L.; Mortensen, K. *Phys. Rev. Lett.* **1994**, *73*, 86.
(27) Matsen, M. W.; Schick, M. *Macromolecules* **1994**, *27*, 6761.
(28) *International Tables of X-ray Crystallography*; Henry, N. F. M., Lonsdale, K., Eds.; Kynoch Press: Birmingham, U.K., 1965; Vol. I. The space group for the hexagonal phase, $p6m$, is found on 372; that of the BCC phase, $Im\bar{3}m$, on 524; that of the HPL phase, $R\bar{3}m$, on 524; and that of the double-gyroid phase, $Ia\bar{3}d$, on 524.

MA9618437